Webology (ISSN: 1735-188X)
Volume 18, Number 6, 2021

Design Of A Cross-Domain Bioinspired Model For Identification Of Gait Components Via Iterated Gans

Ashish Kumar Misal[1a]* , AbhaChaubey[2b] , SiddharthChaubey[2c]

[1a]Computer Science & Engineering Department, RCET Bhilai, India.

[2a]Computer Science & Engineering Department, SSTC Campus Bhilai, India.

[2b]Computer Science & Engineering Department, SSTC Campus Bhilai, India.

Abstract: Gait identification assists in recognition of human body components from temporal image sequences. Such components consist of connected-body entities including head, upper body, lower body regions. Existing Gait recognition models use deep learning methods including variants of Convolutional Neural Networks (CNNs), Q-Learning, etc. But these methods are either highly complex, or do not perform well under complex background conditions. Moreover, most of these models are validated on a specific environmental condition, and cannot be scaled for general-purpose deployments. To overcome these issues, this text proposes design of a novel cross-domain bioinspired model for identification of gait components via Iterated Generative Adversarial Networks (IGANs). The proposed model initially extracts multidomain pixel-level feature sets from different images. These include frequency components via Fourier analysis, entropy components via Cosine analysis, spatial components via Gabor analysis, and window-based components via Wavelet &Convolutional analysis. These feature sets are processed via a Grey Wolf Optimization (GWO) Model, which assists in identification of high-density & highly variant features for different gait components. These features are classified via an iterated GAN, which comprises of Generator & Discriminator ssModels that assist in evaluating connected body components. These operations generate component-level scores that assist in identification of gait from complex background images. Due to which, the proposed model was observed to achieve 9.5% higher accuracy, 3.4% higher precision, and 2.9% higher recall than existing gait identification methods. The model also uses iterative learning, due to which its accuracy is incrementally improved w.r.t. number of evaluated image sets.

Keywords: Gait, Multidomain, Frequency, Entropy, Connected, Body, Components, GAN, Scenarios

1. Introduction

Biometric identification systems have come a long way in recent years. Access control systems and authentication systems are only two examples of where it has been effectively deployed. Behavioural and physiological traits are currently the two primary foci of biometric recognition. Some examples of physical traits include the face, iris, palmprint, and fingerprint. [1, 2, 3, 4], that can be identified via

long short-term memory (LSTM) In order to acquire physiological traits, it is frequently necessary to have physical touch with the target and to have the target's active participation. Gait is a behaviour that may be seen and studied. Without direct touch or even permission from the target, the gait sequence may be recorded. Gait feature extraction, however, may be performed with lower-quality photos or movies. The two most frequent types of gait recognition systems [5, 6] are model-free and model-based. They use Graph Convolutional Neural Network (GCNN) and its counterparts for efficient analysis. With the use of the target's human body model, model-based approaches may extract the static or kinetic aspects of the gait cycle from video recordings. Work in [7]uses the knee and hip's angular motion to create a motion model. Using data on the positions of the joints obtained from a Microsoft Kinect device, a 3D skeleton model is reconstructed to infer the gait characteristics. Unlike model-based approaches, model-free processes don't use body models to extract gait properties from gait sequence silhouettes. Han & Bhanu's Gait Energy Picture (GEP) method takes the many silhouettes that make up a gait cycle and uses them to create a single image by averaging the various forms. There are several variants of GEI that have been suggested, such as Pose Energy Image (PEI) with Self-Adaptive Hidden Markov Model (SA HMM) [8, 9, 10], Frame Difference Energy Image (FDEI) [10], etc. Optical flow-based approaches are another model-free approach [11, 12, 13]. Reconstructing a human body model using Kinect data on its many joints is now a simple task. The Kinect may be used to acquire gait sequences, allowing us to construct a 3D skeleton by recording the 25 (Kinect V2) joint locations [14, 15, 16] in each frame of the gait sequences. In addition, the setting doesn't matter for the walking scenes.

Model-based approaches are used in 3D skeleton-based recognition. Estimation techniques and body sensors/depth cameras like Kinect can provide a rough approximation of the skeleton's shape [17, 18, 19, 20]. There have been three generations of Kinect released thus far. Current state-of-the-art AI sensors, like the Azure Kinect, combine a high-tech depth sensor with a video camera and an orientation sensor. The 3D skeleton may be used to measure static characteristics like height, weight, and bone length. Concurrently accessible kinetic parameters may indicate the dynamic components of the gait sequence.

Autoencoders (AEs) are a kind of artificial neural network that typically have both an encoder and a decoder [21, 22, 23, 24], each of which may be used for certain tasks. They use some form of Ensemble Deep Neural Network (EDNN) for estimation of gait features. Unique property of the autoencoder is that its input data samples serve as the output target. Once the encoder network has been trained using the test data, it may be able to reduce a high-dimensional input to a useful set of low-dimensional vector sequences for usage in real-time applications. Moreover, the results of the many tests show that the encoder's outputs are now more reliable and helpful, particularly when combined with a deep autoencoder under complex imagescenarios.

Models for recognizing gaits now use deep learning techniques like Q-Learning and other kinds of Convolutional Neural Networks (CNN) [25, 26, 27, 28, 29, 30]. These methods, however, are either very sophisticated or fail miserably in more nuanced settings. More importantly, most of these models have only been proven under certain conditions, limiting their applicability. To address these problems, the book suggests constructing a unique cross-domain bioinspired model for recognizing gait

components using iterative generative adversarial networks (IGANs). Some other techniques that identify real-time analysis for other domains are discussed in [31, 32, 33].

Section 3 provides an assessment of the proposed model by comparing it to established methods for gait recognition under situations conceptually similar to those in practice. Conclusions and suggestions for further developing the suggested model for practical use cases.

2. Design of the proposed Cross-Domain Bioinspired Model for identification of Gait Components via Iterated GANs

Existing Gait recognition models employ deep learning techniques, such as variants of Convolutional Neural Networks (CNNs), Q-Learning, etc., based on a review of existing models that perform Gait identification. However, these methods are either extremely complex or have lower performance under complex background conditions. In addition, the majority of these models are validated on a specific environmental condition and cannot be scaled for deployments with a broad scope. This section discusses design of a novel cross-domain bioinspired model for identification of gait components using Iterated Generative Adversarial Networks to address these issues (IGANs). As per the flow of the model in figure 1, it can be observed that initially, the proposed model extracts multidomain pixel-level feature sets from various images. These include frequency components as determined by Fourier analysis, entropy components as determined by Cosine analysis, spatial components as determined by Gabor analysis, and window-based components as determined by Wavelet and Convolutional analysis. These feature sets are processed using the Grey Wolf Optimization (GWO) Model, which facilitates the identification of high-density and highly variant features for various gait components. These features are classified using an iterative GAN consisting of Generator & Discriminator Models, which aid in the evaluation of interconnected body parts. These operations generate component-level scores that aid in identifying gait from images with complex backgrounds.

As per the flow of proposed model, the collected image & video sets are represented via a multidomain feature extraction process. This process initially converts the frames into 1D samples, and extracts Fourier Features via equation 1,

$$DFT_i = \sum_{j=1}^{N_f} x_j * \left[cos\left(\frac{2 * \pi * i * j}{N_f}\right) - \sqrt{-1} * sin\left(\frac{2 * \pi * i * j}{N_f}\right)\right] \dots (1)$$

Where, x are pixel intensity levels, and N_f are total pixels in individual images. This assists in identification of frequency components, which are extended by extraction of entropy components via evaluation of Discrete Cosine Transform (DCT) as per equation 2,

$$F(DCT_i) = \frac{1}{\sqrt{2 * N_f}} * x_i \sum_{j=1}^{N_f} x_j * \cos\left[\frac{\sqrt{-1} * (2 * i + 1) * \pi}{2 * N_f}\right] \dots (2)$$

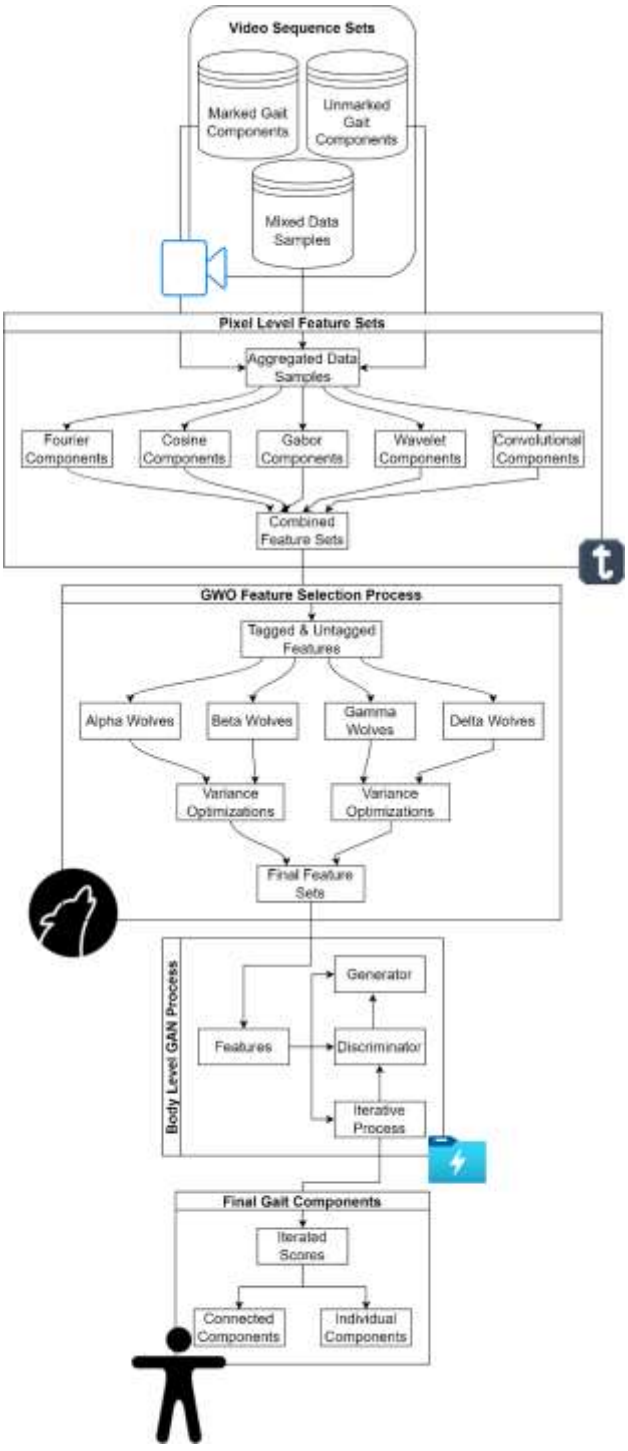

Figure 1. Design of the proposed Gait identification process

These features are cascaded with convolutional features which are extracted as per equation 3,

$$Conv_{out_i} = \sum_{a=-\frac{m}{2}}^{\frac{m}{2}} x(i-a) * LReLU\left(\frac{m+2a}{2}\right) \ldots (3)$$

Where, m & $a$are window & stride dimensions, while $LReLU$is a Leaky Rectilinear Unit that retains only positive feature sets via equation 4,

$$LReLU(x) = l_a * x, when\ x < 0\ , else\ LReLU(x) = x \ldots (4)$$

Where, l_a is a positive scaling constant, that is used to quantize feature sets. The convolutional features are evaluated for different window & stride sizes, which assists in extraction of high-density feature sets. These sets are further extended via a Gabor feature extraction layer, that evaluates angular components via equation 5,

$$G(x,y)_s = e^{\frac{-x`^2+\partial^2*y'^2}{2*\emptyset^2}} * \cos\left(2 * \frac{pi}{\lambda} * x'\right) \ldots (5)$$

Where, ∂ & $\emptyset$ represents 3D angles that are varied in the range of (0, 2π), and assist in identification of orientation feature sets. In equation 5, x, y represents Cartesian value sets, which are estimated as per equation 6,

$$x' = x * \cos(\phi) + y * \sin(\phi)$$
$$y' = -x * \sin(\phi) + y * \cos(\phi) \ldots (6)$$

The Gabor components are useful in identification of pixel-level variations between different Gait components. The variance of this feature vector is aided via extraction of approximate & detailed Wavelet components via equations 7 & 8 as follows,

$$W_a = \frac{x_i + x_{i+1}}{2} \ldots (7)$$

$$W_d = \frac{x_i - x_{i+1}}{2} \ldots (8)$$

When combined, these components form a Gait Feature Vector (GFV), which might contain feature-level redundancies. These redundancies must be reduced in order to improve classification performance, and reduce the delay needed for classification operations. To perform these tasks, a Grey Wolf Optimization (GWO) Model is used, which works as per the following process,

- To setup the GWO process, following constants must be initialized,
  - Count of Wolves that must be reconfigured during the optimization process (N_w)
  - Count of iterations that must be followed for configuration generation (N_i)
  - Rate at which each of the Wolves will be learning from each other (L_w)
- The GWO Model, initially generates these N_w Wolf configurations as per the following process,
  - From the GFV set, select N stochastic features via equation 9,

$$N = STOCH(L_w * N_f, N_f) \dots (9)$$

Where, $STOCH$represents a number generation process that uses Markovian operations.

- Using these features, estimate Wolf fitness as per equation 10,

$$f_w = \sqrt{\frac{\left(\sum_{i=1}^{N}\left(x_i - \sum_{j=1}^{N}\frac{x_j}{N}\right)^2\right)}{N+1}} \dots (10)$$

- Generate N_w such feature configurations.

- Once all configurations are generated, then estimate Wolf fitness threshold via equation 11,

$$f_{th} = \sum_{i=1}^{N_w} f_{w_i} * \frac{L_{w_i}}{N_w} \dots (11)$$

- As per this threshold value, Mark the Wolves via the following process,
  - For Wolves with, $f_w > 2 * f_{th}$, mark them as 'Alpha'
  - For Wolves with,$f_w > f_{th}$, modify its learning rate via equation 12, and mark them as 'Beta',

$$L_w(New) = L_w(Old) + \frac{\sum_{i=1}^{N(Alpha)} L_{w_i}}{N(Alpha)^4} \dots (12)$$

  - For Wolves with$f_w > L_{w_i} * f_{th}$, modify their learning rates as per equation 13, and Mark them as 'Gamma',

$$L_w(New) = L_w(Old) + \frac{\sum_{i=1}^{N(Beta)} L_{w_i}}{N(Beta)^3} \dots (13)$$

  - Other Wolves are marked as 'Delta', and their learning rates are varied as per equation 14,

$$L_w(New) = L_w(Old) + \frac{\sum_{i=1}^{N(Gamma)} L_{w_i}}{N(Gamma)^2} \dots (14)$$

- Repeat the same process for $N_i$iterations, and modify Wolf configurations.

Once all iterations are completed, select all 'Alpha' Wolves, and aggregate their features via equation 15,

$$F(Final) = \bigcup_{i=1}^{N(Alpha)} F_i \dots (15)$$

These final feature sets are processed via an iterative GAN Model, which assists in loss minimization via generator and discriminator processes. The model initially extracts a loss function via equation 16,

$$L(I^t, I^g) = f^g * \log(f^t) + [1 - f^g] * \log(1 - f^t) \dots (16)$$

Where, I^t&$I^g$are the component & non-component image pixels, while,f^t&f^g are their individually selected features. Using this value, estimate maximum loss levels via equation 17,

$$L(Max) = Max[\log(f^t) + \log(1 - f^g)] \dots (17)$$

This loss is minimized via estimation of minimal loss levels via equation 18,

$$L(Min) = Min[\log(f^t) + \log(1 - f^g)] \dots (18)$$

These levels are processed via equation 19, in order to estimate current loss levels,

$$L = Min\big[Max[\log(f^t) + \log(1 - f^g)]\big] \dots (19)$$

A generator probability level is estimated via equation 20, that assists in segregation of body components from non-body components.

$$P(G) = \frac{I^t}{L(Max)} - I^t \dots (20)$$

All the non-body components are removed via estimation of an output probability level as per equation 21,

$$P(out) = E(I^g) * \log\left[\frac{I^t}{0.5 * \big(I^t - P(G)\big)}\right] + E(I^t) * \log\left[\frac{P(G)}{0.5 * \big(I^t - P(G)\big)}\right] \dots (21)$$

Where, $P(Out)$is the probability of pixel belonging to one of the Gait components. Pixels that are processed to similar probability levels are classified as 'Gait' components, while others are classified as 'non-Gait' components. This classification is done as per equation 22, which assists in activating features via Soft Max kernels. This activation allows the model to identify Gait pixels via tuning of weights (w) and bias (b) value sets.

$$P_{out} = SoftMax\left(\sum_{i=1}^{N_f} Conv_{out_i} * w_i + b\right) \dots (22)$$

As per these operations, the proposed model is able to identify Gait components with high efficiency even under complex background conditions. This efficiency can be observed from the next section of this text, where it is compared in terms of accuracy, precision and recall levels with existing gait recognition techniques.

3. Result analysis & comparison

The proposed gait recognition model initially collects different video sets, and represents them via multidomain features. These features include frequency levels, convolutional sets, entropy levels, Gabor sets wavelet sets. The fused features are then processed via an efficient GWO Model, which assists in identification of high inter-class variance features. These classes include 'Gait' and 'non-Gait' categories, which are identified via an iterative GAN Model, that uses Soft Max activation for evaluation of Gait pixels. These evaluations were done on the following datasets,

- NLPR Gait Database (http://www.cbsr.ia.ac.cn/users/szheng/?page_id=71)
- Human Gait Phase Dataset (https://www.kaggle.com/datasets/dasmehdixtr/human-gait-phase-dataset)
- Kinematic Gait Dataset (http://gaitanalysis.th-brandenburg.de/), and
- Human Gait Dataset (https://www.kaggle.com/datasets/drdataboston/93-human-gait-database) samples.

These samples were combined to form a total of 50k image samples, out of which 80% were used to train the GAN Model, while 10% each were used for testing & validation operations. Results of the model on these datasets can be observed from figure 2 (a), 2 (b), and 2 (c), where the model was tested on simpler to complex backgrounds.

Figure 2 (a). Gait identified on simple backgrounds

Figure 2 (b). Gait recognized on slightly complex backgrounds

Figure 2 (c). Gait recognized on complex backgrounds

The results were further compared with LSTM [2], GCNN [5], and EDNN [22] in terms of accuracy (A), precision (P), recall (R), and delay (d) values, which were estimated via equations 23, 24, 25 & 26 as follows,

$$A = \frac{t_p + t_n}{t_p + t_n + f_p + f_n} \dots (23)$$

$$P = \frac{t_p}{t_p + f_p} \dots (24)$$

$$R = \frac{t_p}{t_p + t_n + f_p + f_n} \dots (25)$$

$$d = \frac{1}{N}\sum_{i=1}^{N} t_{end_i} - t_{start_i} \dots (26)$$

Where, $t_p, f_p, t_n \& f_n$ are constants of confusion matrix, while $t_{end} \& t_{start}$ are the timestamps for finishing and starting the classification process. As per this strategy, the accuracy of classification w.r.t. Number of Test Image Sequences (NTIS) can be observed from table 1 as follows,

NTIS	**A (%)** **LSTM [2]**	**A (%)** **GCNN [5]**	**A (%)** **EDNN [22]**	**A (%)** **This Work**

2216	83.24	89.59	91.18	98.91
4450	83.30	89.91	91.37	98.98
6666	83.35	90.23	91.57	99.05
8884	83.40	90.56	91.76	99.10
11116	83.45	90.89	91.97	99.15
13334	83.50	91.23	92.18	99.19
15550	83.56	91.56	92.39	99.23
17784	83.61	91.89	92.61	99.27
20000	83.66	92.22	92.82	99.31
22216	83.71	92.55	93.03	99.36
24450	83.77	92.87	93.24	99.41
27784	83.82	93.20	93.45	99.47
33334	83.87	93.52	93.65	99.54
36116	83.93	93.85	93.85	99.60
38884	83.98	94.17	94.06	99.65
44450	84.03	94.50	94.26	99.70
47216	84.09	94.83	94.47	99.75
50000	84.14	95.16	94.67	99.80

Table 1. Accuracy of Gait identification for different image sets

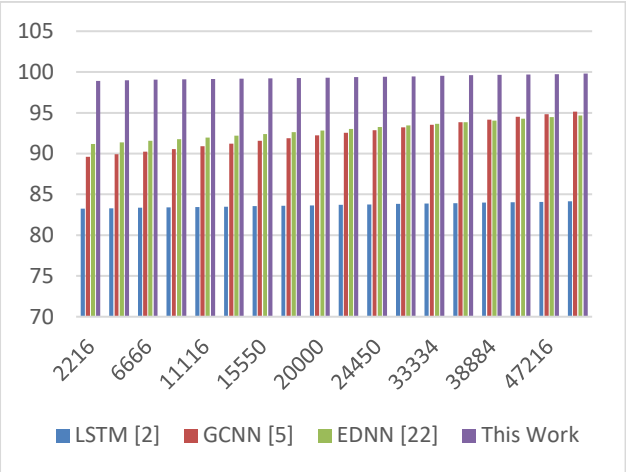

Figure 3. Accuracy of Gait identification for different image sets

Based on this evaluation and figure 3, it can be observed that the proposed model is able to improve Gait identification accuracy by 15.3% when compared with LSTM [2], 5.5% when compared with GCNN [5], and 3.9% when compared with EDNN [22] under real-time image sets. This accuracy is improved due to use of high-density feature sets, and use of GAN which assists in improving the classification performance even under complex backgrounds. Similarly, the precision levels can be observed from table 2 as follows,

NTIS	**P (%)** **LSTM [2]**	**P (%)** **GCNN [5]**	**P (%)** **EDNN [22]**	**P (%)** **This Work**
2216	81.29	85.78	88.17	97.79
4450	81.34	86.09	88.36	97.84
6666	81.39	86.41	88.55	97.89
8884	81.44	86.73	88.74	97.94
11116	81.50	87.05	88.94	97.98
13334	81.55	87.37	89.15	98.02
15550	81.60	87.68	89.35	98.06
17784	81.65	87.99	89.56	98.11

20000	81.71	88.30	89.76	98.16
22216	81.76	88.61	89.96	98.21
24450	81.81	88.91	90.16	98.27
27784	81.86	89.22	90.35	98.33
33334	81.91	89.53	90.54	98.39
36116	81.96	89.84	90.74	98.44
38884	82.01	90.15	90.93	98.50
44450	82.06	90.46	91.13	98.54
47216	82.11	90.78	91.33	98.59
50000	82.16	91.09	91.53	98.64

Table 2. Precision of Gait identification for different image sets

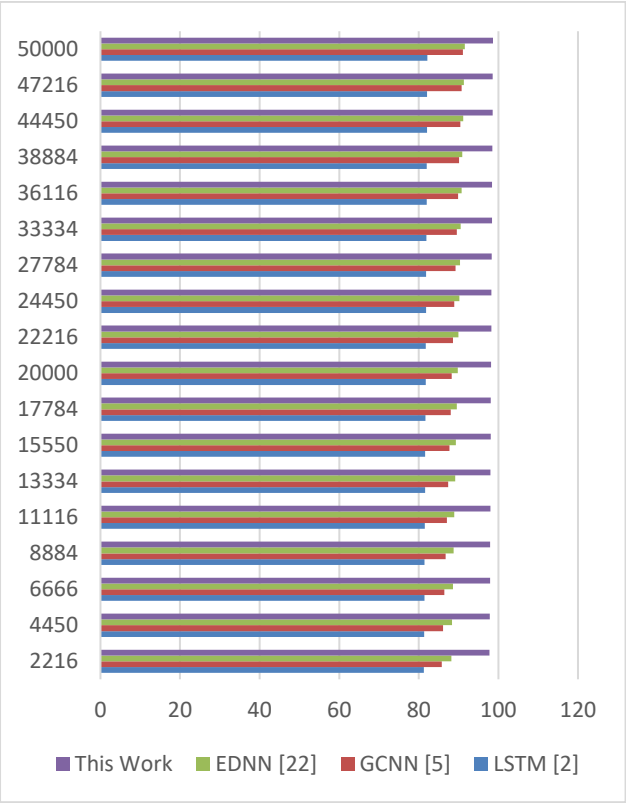

Figure 4. Precision of Gait identification for different image sets

Based on this evaluation and figure 4, it can be observed that the proposed model is able to improve Gait identification precision by 16.2% when compared with LSTM [2], 6.5% when compared with GCNN [5], and 5.9% when compared with EDNN [22] under real-time image sets. This precision is improved due to use of multidomain feature extraction, and use of high efficiency GAN which assists in improving the classification performance even under complex backgrounds. Similarly, the recall levels can be observed from table 3 as follows,

NTIS	**R (%) LSTM [2]**	**R (%) GCNN [5]**	**R (%) EDNN [22]**	**R (%) This Work**
2216	80.28	87.84	88.66	97.16
4450	80.33	88.16	88.85	97.23
6666	80.38	88.48	89.05	97.28
8884	80.44	88.80	89.24	97.33

11116	80.50	89.10	89.44	97.38
13334	80.57	89.39	89.63	97.43
15550	80.65	89.64	89.82	97.49
17784	80.74	89.88	90.01	97.56
20000	80.83	90.11	90.19	97.63
22216	80.92	90.35	90.37	97.71
24450	81.01	90.59	90.55	97.78
27784	81.09	90.84	90.73	97.86
33334	81.17	91.10	90.92	97.94
36116	81.24	91.37	91.10	98.01
38884	81.31	91.66	91.29	98.07
44450	81.38	91.94	91.48	98.13
47216	81.44	92.23	91.67	98.19
50000	81.52	92.50	91.86	98.25

Table 3. Recall of Gait identification for different image sets

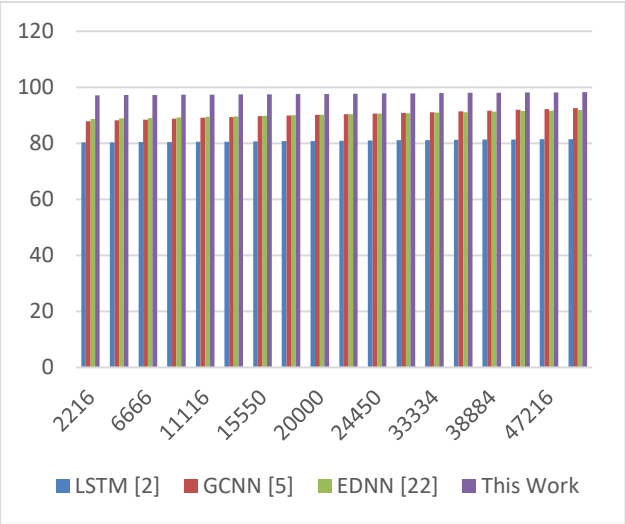

Figure 5. Recall of Gait identification for different image sets

Based on this evaluation and figure 5, it can be observed that the proposed model is able to improve Gait identification recall by 15.9% when compared with LSTM [2], 5.4% when compared with GCNN [5], and 6.3% when compared with EDNN [22] under real-time image sets. This recall is improved due to use of GWO which assists in identification of high-density feature sets, and use of GAN which assists in improving the classification performance even under complex backgrounds. Similarly, the delay needed for identification can be observed from table 4 as follows,

NTIS	**D (ms)** **LSTM [2]**	**D (ms)** **GCNN [5]**	**D (ms)** **EDNN [22]**	**D (ms)** **This Work**
2216	114.24	105.28	107.21	104.95
4450	114.31	105.66	107.44	105.02
6666	114.39	106.05	107.67	105.08
8884	114.46	106.44	107.90	105.13
11116	114.53	106.83	108.14	105.18
13334	114.61	107.22	108.39	105.22
15550	114.68	107.61	108.64	105.26
17784	114.75	108.00	108.89	105.31

20000	114.82	108.38	109.13	105.36
22216	114.90	108.76	109.38	105.41
24450	114.97	109.14	109.62	105.47
27784	115.04	109.52	109.86	105.54
33334	115.12	109.90	110.10	105.60
36116	115.19	110.28	110.34	105.66
38884	115.26	110.66	110.58	105.72
44450	115.34	111.05	110.82	105.77
47216	115.41	111.43	111.06	105.82
50000	115.48	111.82	111.30	105.87

Table 4. Delay needed during Gait identification for different image sets

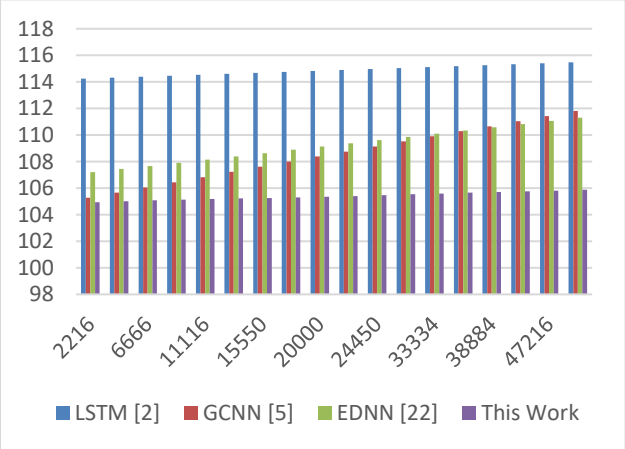

Figure 6. Delay needed during Gait identification for different image sets

Based on this evaluation and figure 6, it can be observed that the proposed model is able to reduce the delay needed for Gait recognition by 10.5% when compared with LSTM [2], 8.3% when compared with GCNN [5], and 8.5% when compared with EDNN [22] under real-time image sets. This delay is reduced due to use of GWO which assists in removal of low variance feature sets, and use of GAN

which assists in improving the classification performance even under complex backgrounds. Due to these enhancements, the proposed model can be used for large-scale gait recognition use cases.

4. Conclusion and future scope

The proposed model for gait recognition initially collects multiple video sets and represents them using multidomain features. These characteristics consist of frequency levels, convolutional sets, entropy levels, Gabor sets, wavelet sets, and wavelet sets. The fused features are then processed using an effective GWO Model, which aids in the identification of features with high inter-class variance. These classes consist of 'Gait' and 'non-Gait' categories, which are determined by an iterative GAN Model that employs Soft Max activation to evaluate Gait pixels. The model improved Gait identification accuracy by 15.3% when compared to LSTM [2], 5.5% when compared to GCNN [5], and 3.9% when compared to EDNN [22] when using real-time image sets. The use of high-density feature sets and GAN, which aids in improving classification performance even with complex backgrounds, contributes to the improvement of this accuracy. In terms of precision levels, it was observed that the proposed model can improve Gait identification precision by 16.2% compared to LSTM [2], 6.5% compared to GCNN [5], and 5.9% compared to EDNN [22] using real-time image sets. This precision is enhanced as a result of the use of multidomain feature extraction and high-efficiency GAN, which improves the classification performance even against complex backgrounds. Consistently, the proposed model improved Gait identification recall by 15.9% when compared to LSTM [2], 5.4% when compared to GCNN [5, and 6.3% when compared to EDNN [22] using real-time image sets. This recall is enhanced as a result of the application of GWO, which aids in the identification of high-density feature sets, and GAN, which aids in improving classification performance even in the presence of complex backgrounds. In terms of operation speed, it was observed that the proposed model can reduce the delay required for Gait recognition by 10.5% when compared to LSTM [2], 8.3% when compared to GCNN [5], and 8.5% when compared to EDNN [22] when using real-time image sets. This delay is reduced as a result of the application of GWO, which aids in the removal of low-variance feature sets, and GAN, which aids in enhancing classification performance even against complex backgrounds. As a result of these enhancements, the proposed model is suitable for large-scale gait recognition applications.

In the future, the proposed model will need to be evaluated on larger image sequences, and its performance can be enhanced through the incorporation of hybrid deep learning models such as Auto Encoders, Transformers, and Q-Learning processes. This efficacy can also be enhanced through bioinspired feature analysis, which enables the model to self-tune its performance in real-time use scenarios.

Conflict of Interest: The authors don’t have any conflict of interest among them.

5. References

[1] Y. Zhang, Y. Huang, S. Yu and L. Wang, "Cross-View Gait Recognition by Discriminative Feature Learning," in IEEE Transactions on Image Processing, vol. 29, pp. 1001-1015, 2020, doi: 10.1109/TIP.2019.2926208.

[2] P. Limcharoen, N. Khamsemanan and C. Nattee, "Gait Recognition and Re-Identification Based on Regional LSTM for 2-Second Walks," in IEEE Access, vol. 9, pp. 112057-112068, 2021, doi: 10.1109/ACCESS.2021.3102936.

[3] Y. Yang, Y. Ge, B. Li, Q. Wang, Y. Lang and K. Li, "Multiscenario Open-Set Gait Recognition Based on Radar Micro-Doppler Signatures," in IEEE Transactions on Instrumentation and Measurement, vol. 71, pp. 1-13, 2022, Art no. 2519813, doi: 10.1109/TIM.2022.3214271.

[4] H. Chao, K. Wang, Y. He, J. Zhang and J. Feng, "GaitSet: Cross-View Gait Recognition Through Utilizing Gait As a Deep Set," in IEEE Transactions on Pattern Analysis and Machine Intelligence, vol. 44, no. 7, pp. 3467-3478, 1 July 2022, doi: 10.1109/TPAMI.2021.3057879.

[5] M. Shopon, G. -S. J. Hsu and M. L. Gavrilova, "Multiview Gait Recognition on Unconstrained Path Using Graph Convolutional Neural Network," in IEEE Access, vol. 10, pp. 54572-54588, 2022, doi: 10.1109/ACCESS.2022.3176873.

[6] X. Ben, C. Gong, P. Zhang, R. Yan, Q. Wu and W. Meng, "Coupled Bilinear Discriminant Projection for Cross-View Gait Recognition," in IEEE Transactions on Circuits and Systems for Video Technology, vol. 30, no. 3, pp. 734-747, March 2020, doi: 10.1109/TCSVT.2019.2893736.

[7] L. Tran, T. Hoang, T. Nguyen, H. Kim and D. Choi, "Multi-Model Long Short-Term Memory Network for Gait Recognition Using Window-Based Data Segment," in IEEE Access, vol. 9, pp. 23826-23839, 2021, doi: 10.1109/ACCESS.2021.3056880.

[8] X. Wang, S. Feng and W. Q. Yan, "Human Gait Recognition Based on Self-Adaptive Hidden Markov Model," in IEEE/ACM Transactions on Computational Biology and Bioinformatics, vol. 18, no. 3, pp. 963-972, 1 May-June 2021, doi: 10.1109/TCBB.2019.2951146.

[9] X. Gu, Y. Guo, F. Deligianni, B. Lo and G. -Z. Yang, "Cross-Subject and Cross-Modal Transfer for Generalized Abnormal Gait Pattern Recognition," in IEEE Transactions on Neural Networks and Learning Systems, vol. 32, no. 2, pp. 546-560, Feb. 2021, doi: 10.1109/TNNLS.2020.3009448.

[10] A. Zhao et al., "Multimodal Gait Recognition for Neurodegenerative Diseases," in IEEE Transactions on Cybernetics, vol. 52, no. 9, pp. 9439-9453, Sept. 2022, doi: 10.1109/TCYB.2021.3056104.

[11] J. Wu, J. Wang, Q. Gao, M. Pan and H. Zhang, "Path-Independent Device-Free Gait Recognition Using mmWave Signals," in IEEE Transactions on Vehicular Technology, vol. 70, no. 11, pp. 11582-11592, Nov. 2021, doi: 10.1109/TVT.2021.3111600.

[12] Y. Yang, L. Chen, J. Pang, X. Huang, L. Meng and D. Ming, "Validation of a Spatiotemporal Gait Model Using Inertial Measurement Units for Early-Stage Parkinson's Disease Detection During Turns," in IEEE Transactions on Biomedical Engineering, vol. 69, no. 12, pp. 3591-3600, Dec. 2022, doi: 10.1109/TBME.2022.3172725.

[13] Y. Xu, W. Yang, M. Chen, S. Chen and L. Huang, "Attention-Based Gait Recognition and Walking Direction Estimation in Wi-Fi Networks," in IEEE Transactions on Mobile Computing, vol. 21, no. 2, pp. 465-479, 1 Feb. 2022, doi: 10.1109/TMC.2020.3012784.

[14] P. Limcharoen, N. Khamsemanan and C. Nattee, "View-Independent Gait Recognition Using Joint Replacement Coordinates (JRCs) and Convolutional Neural Network," in IEEE Transactions on Information Forensics and Security, vol. 15, pp. 3430-3442, 2020, doi: 10.1109/TIFS.2020.2985535.

[15] K. Xu, X. Jiang and T. Sun, "Gait Recognition Based on Local Graphical Skeleton Descriptor With Pairwise Similarity Network," in IEEE Transactions on Multimedia, vol. 24, pp. 3265-3275, 2022, doi: 10.1109/TMM.2021.3095809.

[16] L. Zhang, C. Wang, M. Ma and D. Zhang, "WiDIGR: Direction-Independent Gait Recognition System Using Commercial Wi-Fi Devices," in IEEE Internet of Things Journal, vol. 7, no. 2, pp. 1178-1191, Feb. 2020, doi: 10.1109/JIOT.2019.2953488.

[17] H. Wu, J. Tian, Y. Fu, B. Li and X. Li, "Condition-Aware Comparison Scheme for Gait Recognition," in IEEE Transactions on Image Processing, vol. 30, pp. 2734-2744, 2021, doi: 10.1109/TIP.2020.3039888.

[18] A. Sepas-Moghaddam and A. Etemad, "View-Invariant Gait Recognition With Attentive Recurrent Learning of Partial Representations," in IEEE Transactions on Biometrics, Behavior, and Identity Science, vol. 3, no. 1, pp. 124-137, Jan. 2021, doi: 10.1109/TBIOM.2020.3031470.

[19] L. Zhang, C. Wang and D. Zhang, "Wi-PIGR: Path Independent Gait Recognition With Commodity Wi-Fi," in IEEE Transactions on Mobile Computing, vol. 21, no. 9, pp. 3414-3427, 1 Sept. 2022, doi: 10.1109/TMC.2021.3052314.

[20] R. Liu et al., "A Wearable Gait Analysis and Recognition Method for Parkinson's Disease Based on Error State Kalman Filter," in IEEE Journal of Biomedical and Health Informatics, vol. 26, no. 8, pp. 4165-4175, Aug. 2022, doi: 10.1109/JBHI.2022.3174249.

[21] M. Bukhari et al., "An Efficient Gait Recognition Method for Known and Unknown Covariate Conditions," in IEEE Access, vol. 9, pp. 6465-6477, 2021, doi: 10.1109/ACCESS.2020.3047266.

[22] J. Moon, J. Jung, E. Kang and S. -I. Choi, "Open Set User Identification Using Gait Pattern Analysis Based on Ensemble Deep Neural Network," in IEEE Sensors Journal, vol. 22, no. 17, pp. 16975-16984, 1 Sept.1, 2022, doi: 10.1109/JSEN.2022.3188527.

[23] C. Xu, Y. Makihara, X. Li, Y. Yagi and J. Lu, "Cross-View Gait Recognition Using Pairwise Spatial Transformer Networks," in IEEE Transactions on Circuits and Systems for Video Technology, vol. 31, no. 1, pp. 260-274, Jan. 2021, doi: 10.1109/TCSVT.2020.2975671.

[24] Q. Zou, Y. Wang, Q. Wang, Y. Zhao and Q. Li, "Deep Learning-Based Gait Recognition Using Smartphones in the Wild," in IEEE Transactions on Information Forensics and Security, vol. 15, pp. 3197-3212, 2020, doi: 10.1109/TIFS.2020.2985628.

[25] W. Sheng, F. Zha, W. Guo, S. Qiu, L. Sun and W. Jia, "Finite Class Bayesian Inference System for Circle and Linear Walking Gait Event Recognition Using Inertial Measurement Units," in IEEE Transactions on Neural Systems and Rehabilitation Engineering, vol. 28, no. 12, pp. 2869-2879, Dec. 2020, doi: 10.1109/TNSRE.2020.3032703.

[26] J. Luo and T. Tjahjadi, "View and Clothing Invariant Gait Recognition via 3D Human Semantic Folding," in IEEE Access, vol. 8, pp. 100365-100383, 2020, doi: 10.1109/ACCESS.2020.2997814.

[27] C. Wang, Z. Li and B. Sarpong, "Multimodal adaptive identity-recognition algorithm fused with gait perception," in Big Data Mining and Analytics, vol. 4, no. 4, pp. 223-232, Dec. 2021, doi: 10.26599/BDMA.2021.9020006.

[28] G. Urkude and M. Pandey, "Design and Development of Density-Based Effective Document Clustering Method Using Ontology," Multimed. Tools Appl., Apr. 2022.

[29] X. Chen, X. Luo, J. Weng, W. Luo, H. Li and Q. Tian, "Multi-View Gait Image Generation for Cross-View Gait Recognition," in IEEE Transactions on Image Processing, vol. 30, pp. 3041-3055, 2021, doi: 10.1109/TIP.2021.3055936.

[30] Z. Zhang, L. Tran, F. Liu and X. Liu, "On Learning Disentangled Representations for Gait Recognition," in IEEE Transactions on Pattern Analysis and Machine Intelligence, vol. 44, no. 1, pp. 345-360, 1 Jan. 2022, doi: 10.1109/TPAMI.2020.2998790.

[31] G. Urkude and M. Pandey, "AgriSense: Automatic Irrigation Utility System Using Wireless Sensor Network and Web of Things," in 2019 Second International Conference on Advanced Computational and Communication Paradigms (ICACCP), 2019, pp. 1–6.

[32] G. Urkude and M. Pandey, "AgriOn: A comprehensive ontology for Green IoT based agriculture," J. Green Eng., vol. 10, no. 9, pp. 7078–7101, 2020.

[33] G. Urkude and M. Pandey, "Contextual triple inference using a semantic reasoner rule to reduce the weight of semantically annotated data on fail–safe gateway for WSN," J. Ambient Intell. Humaniz. Comput., Jan. 2021.